

September 5, 2024

PREPARED FOR SUBMISSION TO JCAP

Z' -mediated dark matter freeze-in at stronger coupling

Giorgio Arcadi,^{a,b} David Cabo-Almeida,^{a,b,c,d} Oleg Lebedev^e

^aDipartimento di Scienze Matematiche e Informatiche, Scienze Fisiche e Scienze della Terra,
Universita degli Studi di Messina, Viale Ferdinando Stagno d'Alcontres 31, I-98166 Messina, Italy

^bINFN Sezione di Catania, Via Santa Sofia 64, I-95123 Catania, Italy

^cDepartament de Física Quàntica i Astrofísica, Universitat de Barcelona, Martí i Franquès 1,
E08028 Barcelona, Spain

^dInstitut de Ciències del Cosmos (ICCUB), Universitat de Barcelona, Martí i Franquès 1,
E08028 Barcelona, Spain

^eDepartment of Physics and Helsinki Institute of Physics, Gustaf Hållströmin katu 2a,
FI-00014 Helsinki, Finland

E-mail: giorgio.arcadi@unime.it, david.cabo@ct.infn.it, oleg.lebedev@helsinki.fi

Abstract. We study freeze-in production of fermionic dark matter mediated by a Z' gauge boson. In particular, we explore the regime of Boltzmann-suppressed production, when the Standard Model (SM) thermal bath temperature never exceeds the dark matter mass. The corresponding gauge coupling is then required to be significant, up to order one. As a result, this class of freeze-in models can be probed by the current and future direct dark matter detection experiments.

Contents

1	Introduction	1
1.1	The model	2
2	Dark matter relic abundance	3
2.1	Vector coupling	3
2.2	Axial coupling	5
2.3	Additional channels	5
2.4	Dark matter thermalization	6
3	Constraints and parameter space analysis	7
3.1	LEP constraints	7
3.2	LHC constraints	7
3.3	Direct DM detection	9
3.4	Indirect DM detection	10
3.5	Discussion and summary	10
4	Conclusions	10
A	General cross sections and decay widths	11

1 Introduction

Cosmological dark matter remains one of the most mysterious entities in modern physics. The most common approach to this problem is to postulate the existence of a stable particle which has no quantum numbers with respect to the Standard Model gauge symmetries and whose gravitational effects we observe. Its further properties depend on the coupling to the observed particles as well as itself. If such couplings are very small, the dark matter field never reaches thermal equilibrium and its abundance accumulates over time due to its slow production by the SM thermal bath [1]. This mechanism is known as “freeze-in” [2].

The freeze-in mechanism is predictive only if other production channels are negligible. Generally, there are further non-thermal DM production mechanisms which are operative in the Early Universe [3]. Most importantly, all particles are produced by gravity itself during and after inflation. For example, particle production immediately after inflation, during the inflaton oscillation epoch, can be very efficient due to the presence of the Planck-suppressed operators that couple the inflaton ϕ to DM such as [4, 5]

$$\frac{1}{M_{\text{Pl}}^2} \phi^4 s^2, \quad \frac{1}{M_{\text{Pl}}} \phi^2 \bar{\chi} \chi, \quad (1.1)$$

where s is scalar DM and χ is fermion DM. These operators are generated by both classical and quantum gravitational effects. The resulting abundance of DM exceeds the observed value by many orders of magnitude unless the corresponding Wilson coefficients happen to be very small or DM is extremely light [3].

One way to address this problem is to allow for a long inflaton-dominated expansion period before reheating. The DM quanta produced immediately after inflation are relativistic and their energy density gets diluted by expansion in a non-relativistic background. At the reheating stage, the resulting DM abundance is then small [3]. This implies that the reheating temperature T_R is relatively low, being only limited from below, $T_R > 4$ MeV, by observations [6]. It opens the possibility that the SM bath temperature has never been higher than the DM mass and the freeze-in production is Boltzmann suppressed [7]. The SM-DM coupling required for producing the correct DM relic abundance can then be as large as order one, which facilitates direct searches for dark matter via DM-nucleon scattering and in collider experiments.

The purpose of our current work is to explore this idea in the context of a Z' extension of the Standard Model [8]. The role of dark matter is played by a Dirac fermion which couples to a Z' and whose production by the SM thermal bath is mediated by the Z' . We delineate parameter space leading to the correct DM relic abundance, while satisfying the current direct detection and collider constraints. We find that the Z' -mediated freeze-in can be probed by direct DM detection experiments as long as the Z' has significant “vector” couplings to the SM fermions.

1.1 The model

We study an extension of the Standard Model with a massive Z' boson and a Dirac fermion χ , which has no SM quantum numbers and plays the role of dark matter. The relevant couplings are

$$\mathcal{L} \supset -m_\chi \bar{\chi} \chi - \frac{1}{2} M_{Z'}^2 Z'_\mu Z'^\mu + \bar{\chi} \gamma^\mu (V_\chi - A_\chi \gamma_5) \chi Z'_\mu + \sum_f \bar{f} \gamma^\mu (V_f - A_f \gamma_5) f Z'_\mu, \quad (1.2)$$

Here f represents the SM fermions; $V_{f,\chi}$ and $A_{f,\chi}$ are the vectorial and axial couplings. These are related to the Z' gauge coupling $g_{Z'}$ and the charges of the left- and right-handed fermions X_{f_L}, X_{f_R} as $V_f = g_{Z'}(X_{f_L} + X_{f_R})/2$ and $A_f = g_{Z'}(X_{f_L} - X_{f_R})/2$.

We assume that the Z' is the only portal between the SM and dark matter, focussing on the TeV scale $M_{Z'}$. We also take its mixing with the SM gauge bosons to be negligible for our purposes. The U(1) extensions of the SM are subject to the anomaly cancellation constraint, which generally necessitates the presence of additional fermions. Such fermions, however, can be vector-like with respect to the SM gauge charges and hence have large masses making their impact on the DM phenomenology insignificant. A similar approach was taken in related work [9, 10] (see also [11]).

In what follows, we study freeze-in production of dark matter χ mediated by the Z' . Our main assumption is that the SM thermal bath temperature T is always below m_χ . This means, in particular, that the reheating temperature T_R is sufficiently low, allowing for dilution of the gravitationally produced relics, as explained above. To compute the DM production, we resort to the instant reheating approximation, e.g. take T to increase abruptly from zero to T_R and then decrease as usual, in accordance with the SM entropy conservation. This gives a good estimate of the DM abundance in cosmological models with a flat SM temperature profile before reheating [12]. Using appropriate rescaling and replacing T_R with the maximal SM sector temperature, we can extend our results to a broader class of models. Earlier work on the Z' -mediated freeze-in, which assumes a high reheating temperature, can be found in [13].

2 Dark matter relic abundance

In this section, we study freeze-in dark matter production in the Boltzmann-suppressed regime $T \ll m_\chi$. Dark matter is produced via annihilation of the SM thermal bath particles, e.g. $\bar{f}f \rightarrow Z' \rightarrow \bar{\chi}\chi$, and its density $n = n_\chi + n_{\bar{\chi}}$ is controlled by the Boltzmann equation,

$$\dot{n} + 3Hn = 2\Gamma(\text{SM} \rightarrow \bar{\chi}\chi) - 2\Gamma(\bar{\chi}\chi \rightarrow \text{SM}) , \quad (2.1)$$

where the factor of 2 accounts for production of 2 DM states, χ and $\bar{\chi}$, and Γ is the reaction rate per unit volume.

Since dark matter is non-relativistic at $T \ll m_\chi$, the $a \rightarrow b$ reaction rate is given by

$$\Gamma_{a \rightarrow b} = \int \left(\prod_{i \in a} \frac{d^3 \mathbf{p}_i}{(2\pi)^3 2E_i} f(p_i) \right) \left(\prod_{j \in b} \frac{d^3 \mathbf{p}_j}{(2\pi)^3 2E_j} \right) |\mathcal{M}_{a \rightarrow b}|^2 (2\pi)^4 \delta^4(p_a - p_b) , \quad (2.2)$$

where p_i and p_j are the initial and final state momenta, respectively, and $f(p)$ is the momentum distribution function. $\mathcal{M}_{a \rightarrow b}$ is the QFT $a \rightarrow b$ transition amplitude, in which both the initial and final state phase space symmetry factors are absorbed. For the $2 \rightarrow 2$ reactions, energy conservation combined with the Boltzmann statistics $f(p) = e^{-E/T}$ implies

$$f(p_1)f(p_2) = f(p_3)f(p_4) . \quad (2.3)$$

Therefore, the DM production rate via thermal SM states can be written as the *thermal* DM annihilation rate into SM quanta,

$$\Gamma(\text{SM} \rightarrow \bar{\chi}\chi) = \Gamma(\bar{\chi}\chi|_{\text{therm}} \rightarrow \text{SM}) . \quad (2.4)$$

The latter can be computed following Gelmini and Gondolo [14],

$$\begin{aligned} \Gamma(\bar{\chi}\chi|_{\text{therm}} \rightarrow \text{SM}) &= \langle \sigma(\bar{\chi}\chi|_{\text{therm}} \rightarrow \text{SM}) v_r \rangle n_\chi n_{\bar{\chi}} = \frac{2^2}{(2\pi)^6} \int \sigma v_r e^{-E_1/T} e^{-E_2/T} d^3 p_1 d^3 p_2 \\ &= \frac{2^3 \pi^2 T}{(2\pi)^6} \int_{4m_\chi^2}^{\infty} ds \sigma(s - 4m_\chi^2) \sqrt{s} K_1(\sqrt{s}/T) , \end{aligned} \quad (2.5)$$

where σ is the $\bar{\chi}\chi \rightarrow \text{SM}$ cross section; v_r is the relative velocity of the colliding quanta with energies E_1, E_2 and momenta p_1, p_2 ; n_χ is the χ number density; $\langle \dots \rangle$ denotes a thermal average; s is the Mandelstam variable, and $K_1(x)$ is the modified Bessel function of the first kind. We have explicitly factored out the spin d.o.f. factor 2^2 specific to fermion annihilation ($n_\chi = 2e^{-E/T}$).

Let us focus for now on a heavy Z' regime, $M_{Z'} > 2m_\chi$. It is instructive to consider in detail the limit $M_{Z'} \gg m_\chi, m_f$, where f represents the SM fermions. This allows us to obtain simple analytical approximations in the pure freeze-in limit. In our numerical studies however, we do not resort to this approximation and use the exact (tree-level) results together with the backreaction term in (2.1). In what follows, we consider the vector and axial Z' cases separately.

2.1 Vector coupling

In most of the parameter space, the main production/annihilation channel is

$$\bar{\chi}\chi \leftrightarrow \bar{f}f , \quad (2.6)$$

where f is an SM fermion and contributions of all the fermions lighter than χ should be summed. The DM annihilation via a vector Z' is allowed already at the s -wave level and the corresponding cross section for $m_\chi \gg m_f$ is

$$\sigma(\bar{\chi}\chi \rightarrow \bar{f}f) \simeq \frac{V_f^2 V_\chi^2 m_\chi^2}{2\pi M_{Z'}^4} \sqrt{\frac{s}{s - 4m_\chi^2}}. \quad (2.7)$$

The reaction rate is found from Eq. 2.5. In the regime $m_\chi \gg T$, we may use the asymptotic form $K_1(\sqrt{s}/T) \simeq \sqrt{\frac{\pi}{2}} \frac{T^{1/2}}{s^{1/4}} e^{-\sqrt{s}/T}$. When computing the integral over s , one can use the following approximation: since the integrand peaks sharply close to $s = 4m_\chi^2$, one may replace $s \rightarrow 4m_\chi^2$ in “slow” functions of s , while keeping the factors $\sqrt{s - 4m_\chi^2}$ and $e^{-\sqrt{s}/T}$ as they are. The resulting integral reduces to the Gamma function such that

$$\int_{4m_\chi^2}^{\infty} ds \sqrt{s - 4m_\chi^2} e^{-\sqrt{s}/T} \simeq \frac{\sqrt{\pi}}{2} (4m_\chi T)^{3/2} e^{-2m_\chi/T}. \quad (2.8)$$

The resulting DM production rate via SM fermion annihilation according to (2.4) is

$$\Gamma(\bar{f}f \rightarrow \bar{\chi}\chi) = \frac{V_f^2 V_\chi^2 m_\chi^5 T^3}{2\pi^4 M_{Z'}^4} e^{-2m_\chi/T}. \quad (2.9)$$

In the pure freeze-in regime, the Boltzmann equation (2.1) reduces to $\dot{n} + 3nH = 2\Gamma(\bar{f}f \rightarrow \bar{\chi}\chi)$. It can be solved analytically for simple reheating scenarios. For definiteness, we resort to the instant reheating approximation, that is, we assume that the SM sector temperature increases abruptly from zero to T_R . After that it is determined by entropy conservation, as usual. Integrating the Boltzmann equation from $T = T_R$ to $T = 0$, one finds that $n \propto T^3$ at late times and, due to the exponential suppression of the reaction rate, the production is dominated by the initial moments when $T \simeq T_R$. Using

$$s_{\text{SM}} = \frac{2\pi^2}{45} g_* T^3, \quad H = \sqrt{\frac{g_* \pi^2}{90}} \frac{T^2}{M_{\text{Pl}}}, \quad (2.10)$$

where g_* is the effective number of the SM d.o.f. and $M_{\text{Pl}} = 2.4 \times 10^{18} \text{ GeV}$, we find

$$Y \equiv \frac{n}{s_{\text{SM}}} \simeq \sum_f \frac{45\sqrt{90}}{4} \frac{V_f^2 V_\chi^2}{\pi^7 g_*^{3/2}} \frac{m_\chi^4 M_{\text{Pl}}}{M_{Z'}^4 T_R} e^{-2m_\chi/T_R}, \quad (2.11)$$

where the sum runs over all SM Dirac fermions f with the color multiplicity properly included.¹ Here we have assumed that g_* stays approximately constant in the regime of interest. For the universal couplings $V_f = V_\chi = \lambda$, the observed $Y = 4.4 \times 10^{-10} \text{ GeV}/m_\chi$ requires

$$\lambda \simeq 10^{-6} \frac{M_{Z'} T_R^{1/4}}{m_\chi^{5/4}} e^{m_\chi/(2T_R)} \quad (2.12)$$

for $g_* \simeq 107$. Since $m_\chi \gg T_R$, the exponential factor can be large making λ as large as $\mathcal{O}(1)$. Nevertheless, the produced dark matter density is low and it does not thermalize, thereby justifying

¹The neutrinos contribute 1/2 of the Dirac fermion contribution. For $V_f = V_\chi = \lambda$ and $m_\chi > m_t$, the sum over all the SM fermions amounts to a factor of 22.5.

the assumption of the freeze-in regime. We note that the size of the coupling is determined primarily by m_χ/T_R and is rather insensitive to a specific charge assignment, thus making the universal charge limit justified.

The above result is obtained in the instant reheating approximation. As shown in [12], this gives a good estimate of the required coupling within a larger class of models. If the SM temperature is constant before reheating, Eq. 2.12 stands as it is, up to a small (percent level) shift in T_R . More generally, DM production peaks at the maximal temperature T_{\max} such that one replaces $T_R \rightarrow T_{\max}$ in the above formulas and, to account for entropy production between $T = T_{\max}$ and $T = T_R$, rescales the coupling with the factor $(T_R/T_{\max})^\kappa$, where κ is model dependent.

The common feature of freeze-in models at stronger coupling is that the DM abundance exhibits the factor e^{-2m_{DM}/T_R} times some power of the dark matter coupling [15, 16]. As in the other models, we find that an order one coupling requires $m_{\text{DM}} \sim 20 T_R$ for typical parameter values.

2.2 Axial coupling

Consider now DM production via $\bar{f}f \rightarrow \bar{\chi}\chi$ mediated by an axial Z' [10]. To compute the reaction rate, we consider non-relativistic DM annihilation. In contrast to the previous case, in the $m_f \rightarrow 0$ limit, the process is p -wave and hence less efficient. Neglecting the fermion masses, one finds

$$\sigma(\bar{\chi}\chi \rightarrow \bar{f}f) \simeq \frac{A_f^2 A_\chi^2}{12\pi M_{Z'}^4} \sqrt{s(s - 4m_\chi^2)}. \quad (2.13)$$

This approximation applies for heavy DM, $m_\chi \gg m_t$, or in the regime where the top-quark channel is not available, $m_\chi < m_t$. The reaction rate calculation proceeds as before, except the different velocity dependence leads to the integral

$$\int_{4m_\chi^2}^{\infty} ds (s - 4m_\chi^2)^{3/2} e^{-\sqrt{s}/T} \simeq \frac{3\sqrt{\pi}}{4} (4m_\chi T)^{5/2} e^{-2m_\chi/T} \quad (2.14)$$

instead of (2.8). The result is

$$\Gamma(\bar{f}f \rightarrow \bar{\chi}\chi) = \frac{A_f^2 A_\chi^2 m_\chi^4 T^4}{2\pi^4 M_{Z'}^4} e^{-2m_\chi/T}. \quad (2.15)$$

Note that the rate is now proportional to T^4 , unlike that in the vector case. The DM abundance is given by

$$Y \simeq \sum_f \frac{45\sqrt{90}}{4} \frac{A_f^2 A_\chi^2}{\pi^7 g_*^{3/2}} \frac{m_\chi^3 M_{\text{Pl}}}{M_{Z'}^4} e^{-2m_\chi/T_R}. \quad (2.16)$$

For $A_f = A_\chi = \lambda$ and $g_* \simeq 107$, the required coupling is

$$\lambda \simeq 10^{-6} \frac{M_{Z'}}{m_\chi} e^{m_\chi/(2T_R)}. \quad (2.17)$$

2.3 Additional channels

For heavier DM, $m_\chi \sim M_{Z'}$, the decay and t -channel processes

$$Z' \rightarrow \bar{\chi}\chi, \quad Z'Z' \rightarrow \bar{\chi}\chi \quad (2.18)$$

become important. The Z' number density receives Boltzmann suppression similar to $e^{-2m_\chi/T}$, hence processes with the Z' on-shell cannot be neglected. The Z' gauge boson maintains thermal equilibrium with the SM bath due to its coupling to light fermions. The reaction

$$\bar{f}f \leftrightarrow Z' \quad (2.19)$$

is very efficient for the coupling range of interest and faster than the rate of expansion of the Universe (see e.g. analogous calculations in [16]), thereby implying thermal equilibrium.

The decay channel $Z' \rightarrow \bar{\chi}\chi$ dominates around $M_{Z'} \sim 2m_\chi$, while the efficiency of the t -channel mode $Z'Z' \rightarrow \bar{\chi}\chi$ depends on the nature of the Z' couplings. In case of the axial couplings, the fermion annihilation mode is suppressed by m_f or DM velocity. On the other hand, the processes involving the longitudinal component of a Z' at high energy are enhanced by $E/M_{Z'}$. Hence, one expects $Z'Z' \rightarrow \bar{\chi}\chi$ to dominate for large m_χ . Fig. 1 (left) shows the relative reaction rate contributions of the different production channels for the axial coupling case, produced with `micrOMEGAs` [17, 18]. As expected, we observe that the t -channel annihilation becomes dominant for heavy dark matter. In the vector coupling case, on the other hand, the SM fermion annihilation mode is efficient and we find that it remains the main production channel at large m_χ .

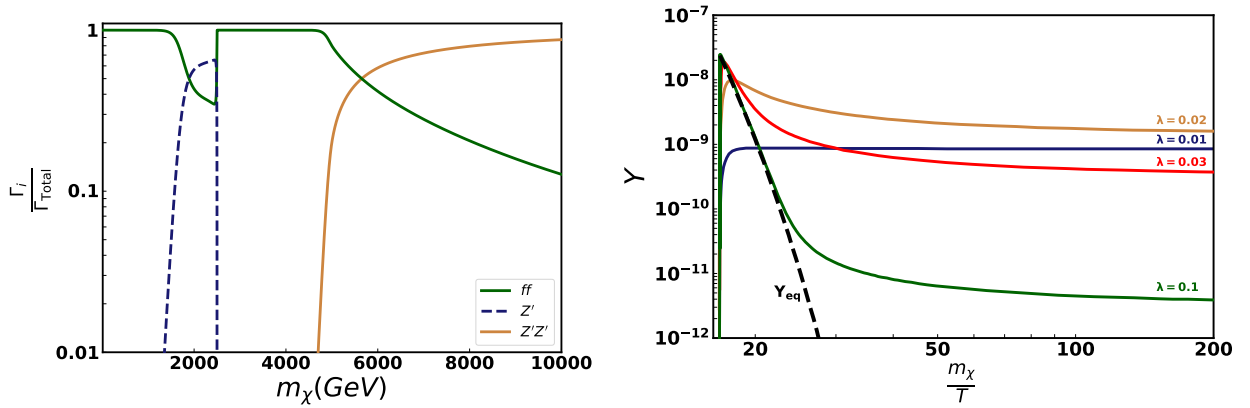


Figure 1: *Left:* Dark matter production relative contributions $\Gamma_i/\Gamma_{\text{tot}}$ for the s -channel, t -channel and decay reactions. Here the *axial* coupling is assumed: $A_f = A_\chi = 0.1$ ($V_f = V_\chi = 0$); $M_{Z'} = 5$ TeV and $T_R = 120$ GeV. *Right:* Evolution of the DM abundance Y for different couplings. Here $m_\chi = 300$ GeV, $M_{Z'} = 900$ GeV and $T_R = 18$ GeV; the coupling is defined by $\lambda = V_f = V_\chi = A_f = A_\chi$. Y_{eq} represents the thermal equilibrium value.

2.4 Dark matter thermalization

The above considerations help us understand the qualitative behaviour of $\lambda(m_\chi, T_R)$ at low DM densities, when the term $\Gamma(\bar{\chi}\chi \rightarrow \text{SM})$ in Eq. 2.1 can be neglected. However, in our numerical analysis we use the `micrOMEGAs` tool [17, 18] which takes into account all the channels as well as the DM annihilation effects. The latter lead to a qualitative change in the relic abundance calculations at larger coupling. As one increases λ , the DM density grows thus enhancing DM annihilation and eventually leading to its thermalization. This manifests itself in the freeze-in lines $\lambda(m_\chi, T_R)$ merging with the freeze-out curve $\lambda(m_\chi)$, as we show in the next section. Such thermalization has been studied in detail in [7] and entails a smooth FIMP-WIMP transition [19].

Fig. 1 (right) illustrates the effect of the coupling increase on the eventual DM abundance. While at small λ , Y grows with the coupling, this ceases to be the case above a certain critical coupling, which is around $\lambda \sim 0.02$ in this example. We observe that the abundance decreases over time due to DM annihilation. At yet larger couplings, $Y(T)$ follows its equilibrium value $Y_{\text{eq}}(T)$ for an extended period of time, before freeze-out. This signals DM thermalization.

We note that, in order to compute $\Gamma(\bar{\chi}\chi \rightarrow \text{SM})$, one needs to know the momentum distribution of dark matter. This reaction becomes important at large enough coupling and, thus, it is safe to assume that the SM-DM system is in kinetic equilibrium at that stage. Indeed, the elastic scattering reaction $\text{SM}+\chi \rightarrow \text{SM}+\chi$ is more efficient than the annihilation one due to the higher density of the SM states. Hence, kinetic equilibrium sets in at smaller couplings. This is also the assumption adopted in `micrOMEGAs`.

3 Constraints and parameter space analysis

In this section, we delineate parameter space of the model producing the correct DM relic abundance and discuss various constraints on the “universal” coupling λ . These include bounds on the Z' interactions from collider experiments as well as constraints on dark matter from direct and indirect searches.

3.1 LEP constraints

A heavy Z' can be integrated out leading to a set of 4-fermion interactions. The strictest constraints on the contact interactions are imposed by the 4-lepton operators $\ell\ell\ell\ell$, while the lepton-quark operators $\ell\ell qq$ [20] are less important. The most significant observables are the muon decay constant, which is affected by the muon-electron operators, as well as the LEP lepton measurements [21, 22]. The relevant constraints for the flavor-universal case can be read off from Fig. 3 (right) of [23]. The vector coupling ($\kappa_L = \kappa_R$) is constrained by

$$\frac{\lambda}{M_{Z'}} < \frac{0.12}{\text{TeV}} \quad (3.1)$$

at 95 % CL. The constraint on the axial coupling ($\kappa_L = -\kappa_R$) is somewhat weaker,

$$\frac{\lambda}{M_{Z'}} < \frac{0.19}{\text{TeV}} \quad (3.2)$$

at 95 % CL. The corresponding excluded regions are shown in Fig. 2 in light orange, marked “LEP”.

3.2 LHC constraints

The LHC experiments are conducting direct searches for a new gauge boson Z' in the channel $pp \rightarrow \ell^+\ell^-X$, where X represents the beam fragment jets. The constraints are obtained on the quantity $\sigma(pp \rightarrow Z') \text{BR}(Z' \rightarrow \ell^+\ell^-)$, employing the narrow width approximation. We use the current data from ATLAS [24] based on LHC Run 2 at $\sqrt{s} = 13$ TeV with a total integrated luminosity of $L = 139 \text{ fb}^{-1}$. The theory prediction for $\sigma(pp \rightarrow Z')$ is computed using MadGraph [25]. As the first step, we reproduce the ATLAS limits on the Z'_ψ model [24]. Then, we derive the bounds on the universal coupling λ in our model. The results are presented in Fig. 2: the light blue area marked $Z' \rightarrow \ell\ell$ is excluded by the LHC.

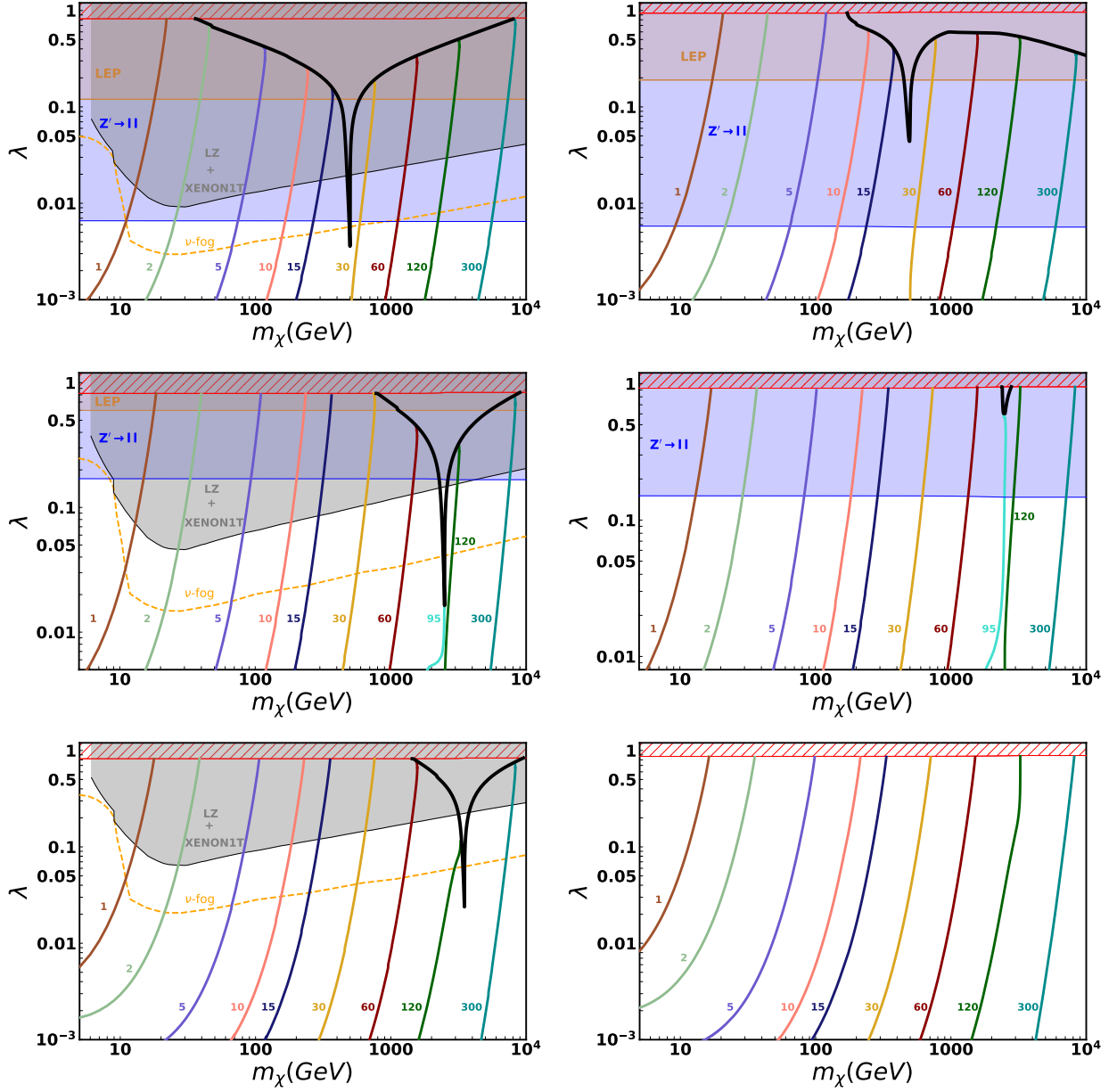


Figure 2: Allowed vector and axial Z' couplings for different $M_{Z'}$. *Top:* $M_{Z'} = 1$ TeV; *Middle:* $M_{Z'} = 5$ TeV; *Bottom:* $M_{Z'} = 7$ TeV. The *left* panels correspond to the vector couplings $V_f = V_\chi = \lambda$ (and $A_f = A_\chi = 0$), while the *right* panels correspond to the axial couplings $A_f = A_\chi = \lambda$ (and $V_f = V_\chi = 0$). Along the colored curves labelled by T_R (in GeV), the correct DM relic density is reproduced. The black line corresponds to thermal DM undergoing freeze-out. The shaded areas are excluded and the “ ν -fog” curve represents the neutrino background for the direct DM detection experiments.

The typical bound on the Z' mass for the SM-like couplings is around 5 TeV [24, 26]. The constraint fades away very fast as $M_{Z'}$ increases and above 6-7 TeV the LHC has no sensitivity to the extra gauge boson, at least at the perturbative level. This is unlike the other bounds (LEP,

direct DM detection) which scale as a function of $\lambda/M_{Z'}$.

3.3 Direct DM detection

Direct DM detection experiments traditionally set the strongest constraints on dark matter models (see, e.g. a recent discussion in [27]). These are based on non-observation of any significant interaction of dark matter with nucleons. In our case, such an interaction is mediated by the Z' . The DM-nucleon scattering occurs at low energy, hence the Z' can be integrated out resulting in the effective Lagrangian

$$\mathcal{L}_{\text{eff}} \supset \frac{1}{M_{Z'}^2} \left[V^\chi \left(2V^u + V^d \right) \bar{\chi} \gamma^\mu \chi \bar{p} \gamma_\mu p \right. \quad (3.3)$$

$$\left. + A^\chi \left(\Delta_u^p A^u + (\Delta_d^p + \Delta_s^p) A^d \right) \bar{\chi} \gamma^\mu \gamma^5 \chi \bar{p} \gamma_\mu \gamma^5 p \right], \quad (3.4)$$

where p represents the proton, and a similar expression applies to the neutron n . $\Delta_i^{p,n}$ stands for the spin content of quark i in the proton/neutron. According to [28],

$$\Delta_u^p = 0.842, \quad \Delta_d^p = -0.427, \quad \Delta_s^p = -0.085, \quad (3.5)$$

and the corresponding neutron quantities are obtained by the isospin symmetry. The resulting cross section for spin-independent scattering of DM on a nucleus with charge Z and atomic weight A is

$$\sigma_{\chi N}^{\text{SI}} = \frac{\mu_{\chi N}^2 (V^\chi)^2}{\pi M_{Z'}^4} \left[V^u \left(1 + \frac{Z}{A} \right) + V^d \left(2 - \frac{Z}{A} \right) \right]^2, \quad (3.6)$$

where $\mu_{\chi N}$ is the reduced mass of the DM-nucleon system. This cross section must lie below the LZ 2022 and XENON1T bounds [29, 30], which imposes a significant constraint on the model parameters. For the case of the universal coupling λ , the direct detection constraint scales as $\lambda^4/M_{Z'}^4$, while $\sigma_{\chi N}^{\text{SI}}$ remains independent of the DM mass as long as $m_\chi \gg 1$ GeV.

The axial couplings lead to the spin-dependent DM-nucleon scattering, which is only weakly constrained and the resulting bounds are unimportant for our analysis. The LHC searches impose the leading constraints in this case, at least for the $M_{Z'}$ range of interest.

In Fig. 2, we show the direct detection constraints on the universal coupling λ with the help of the `micrOMEGAs` tool. The grey regions marked by “LZ+XENON1T” are excluded.² We observe that for a heavy Z' , these constraints supersede the other bounds, while for a lighter Z' , the LHC searches set the strictest bounds. The figures also display the “neutrino fog” which represents the neutrino background for the direct DM detection experiments [31]. The standard techniques would not be able to distinguish the DM scattering from that of neutrinos, if λ falls below the neutrino fog curve. While the corresponding parameter space could be explored with innovative techniques, DM detection is challenging for such low couplings. Nevertheless, we see that large regions of the freeze-in parameter space, especially for a heavy Z' , lie above the neutrino background and thus can be probed by the current and future direct DM detection experiments such as XENONnT [32] and DARWIN [33].³

²The LZ collaboration has updated its 2022 direct detection bound. According to the preliminary (unpublished) estimate, the bound has improved by a factor of 5 - 10, depending on the DM mass. This translates into a stronger constraint on λ by a factor of 1.5 - 1.8.

³This property is shared by a class of freeze-in models with a light mediator [34, 35] as well as the Higgs-portal-type WIMP models with a first order phase transition [36].

3.4 Indirect DM detection

Indirect dark matter detection is based on possible signatures of its annihilation in regions with significant DM density, e.g. the Galactic center. The strictest bounds come from the Fermi-LAT [37] observation of 30 dSphs for 14.3 years. Interpreting these constraints in our model using `micrOMEGAs`, we find that they are superseded by the bounds discussed above and thus are insignificant.

3.5 Discussion and summary

The correct DM relic abundance is reproduced along the colored lines in Fig. 2. Each of them has a different reheating temperature T_R , which we also identify with the maximal SM bath temperature. We observe that, at sufficiently large coupling, all the freeze-in lines merge with the thermal black curve. This signals DM thermalization such that the relic abundance is controlled by the usual freeze-out. The corresponding parameter space is, however, ruled out experimentally, leaving only a very narrow resonance region $m_\chi \simeq M_{Z'}/2$.

In addition to the constraints discussed above, we impose the perturbativity bound which excludes the red hatched area. In this region, the Z' resonance becomes too broad such that $\Gamma_{Z'} > 0.5 M_{Z'}$ and it ceases to be a “particle” in the conventional sense. While for a light Z' this bound is superseded by other constraints, in the case of a heavy Z' , it becomes important, especially for the axial-type couplings.

The axial coupling case is constrained mostly by collider observables, whereas the direct detection bounds are very weak. This also implies that an axial Z' -induced freeze-in can hardly be probed experimentally. On the other hand, the vector case is more interesting and significant parts of the freeze-in parameter space can be probed by the direct detection experiments. For $M_{Z'} = 1$ TeV, the LHC constraints dominate, yet they leave a modestly sized region above the ν -fog line, which can therefore be probed by direct DM detection. The size of this area grows as $M_{Z'}$ increases and at $M_{Z'} = 7$ TeV, the LHC bounds fade away.

We observe that, as long as the Z' couplings have a significant vector component, the direct DM detection prospects are good in the entire range of the DM mass considered, $10 - 10^4$ GeV. The required gauge coupling is in the range $10^{-3} - 10^{-1}$ for a Z' mass between 1 and 10 TeV.

4 Conclusions

We have analyzed Z' -mediated fermion dark matter production in the freeze-in regime at stronger coupling, when the SM bath temperature is below the DM mass. Models with a low reheating temperature are motivated by the problem of gravitational particle production which mars the usual freeze-in mechanism. In particular, Planck-suppressed operators coupling dark matter to the inflaton are very efficient in particle production immediately after inflation, which leads to a large initial abundance of dark matter. This problem can be solved by allowing for an extended period of inflaton-dominated expansion thereby diluting the initial DM abundance. As a result, the reheating temperature in this framework is relatively low, depending on further details.

Using both analytic estimates and more sophisticated numerical tools, we find that the correct DM relic abundance can be produced for a broad range of the DM mass m_χ , assuming a TeV-scale Z' . The main factor is the reheating temperature T_R and, for $m_\chi/T_R \sim 20$, the Z' couplings can be as large as $\mathcal{O}(1)$. We distinguish the vector and axial coupling cases, which exhibit different phenomenology. While the DM production rates are similar in both cases, the constraints on the

parameter space differ substantially. In particular, the direct DM detection results set strict bounds on the vector coupling, whereas the axial coupling remains essentially unconstrained. In our freeze-in framework, this implies that the vector case can be probed by the current and future direct detection experiments, which will reach the sensitivity at the level of the “neutrino fog”. The axial case, on the other hand, is very difficult to test due to the suppression of the DM-nucleus cross section. Further bounds on the parameter space are imposed by the direct Z' searches at the LHC, LEP measurements of the lepton production and constraints from the muon decay.

As the Z' coupling increases, the DM production grows more efficient and the inverse reaction becomes significant. At some critical value of the coupling (depending on T_R), both reactions equilibrate and dark matter thermalizes. We observe this explicitly as the freeze-in relic abundance curves merge with the standard freeze-out line. In the vector coupling case, the corresponding region of the parameter space is ruled out by the direct DM detection. However, at lower couplings, the Boltzmann-suppressed freeze-in is still operative and produces the correct relic abundance while evading such constraints. For a range of the vector couplings, typically of order $10^{-3} - 10^{-1}$, the DM-nucleon cross section lies above the neutrino fog and thus can be tested in the near future. Needless to say, this does not require the Z' to be purely “vectorial”, it only sets a lower bound on the vector component of the Z' coupling.

Our main conclusion is that, as long as the vector coupling of the Z' is substantial, the freeze-in dark matter can be probed further (and possibly discovered) by direct DM detection experiments such as XENONnT and DARWIN.

Acknowledgments

The authors thank Francesco Costa for fruitful discussions. D.C.A. acknowledges funding from the Spanish MCIN/AEI/10.13039/501100011033 through grant PID2022-136224NB-C21.

A General cross sections and decay widths

In this appendix, we provide some analytical formulas for the general case of the vector and axial couplings being present simultaneously. The DM annihilation cross section into a Standard Model Dirac fermion f is given by

$$\begin{aligned} \sigma_{\bar{\chi}\chi \rightarrow \bar{f}f} = & \frac{1}{12\pi s \left[(s - M_{Z'}^2)^2 + M_{Z'}^2 \Gamma_{Z'}^2 \right]} \sqrt{\frac{1 - 4m_f^2/s}{1 - 4m_\chi^2/s}} \left[A_f^2 V_\chi^2 (s - 4m_f^2) (2m_\chi^2 + s) \right. \\ & + A_f^2 A_\chi^2 \left(4m_\chi^2 \left[m_f^2 \left(7 - \frac{6s}{M_{Z'}^2} + \frac{3s^2}{M_{Z'}^4} \right) - s \right] + s (s - 4m_f^2) \right) \\ & \left. + V_f^2 (2m_f^2 + s) (A_\chi^2 (s - 4m_\chi^2) + V_\chi^2 (2m_\chi^2 + s)) \right] , \end{aligned} \quad (\text{A.1})$$

where s is the Mandelstam variable. This result agrees with the corresponding cross section presented in [38]. The Z' decay width is

$$\Gamma_{Z'} = \Gamma_{Z' \rightarrow \bar{\chi}\chi} + \sum_f \Gamma_{Z' \rightarrow \bar{f}f} , \quad (\text{A.2})$$

with

$$\Gamma_{Z' \rightarrow \bar{\chi}\chi} = \frac{\sqrt{M_{Z'}^2 - 4m_\chi^2} \left(A_\chi^2 (M_{Z'}^2 - 4m_\chi^2) + V_\chi^2 (2m_\chi^2 + M_{Z'}^2) \right)}{12\pi M_{Z'}^2} , \quad (\text{A.3})$$

$$\Gamma_{Z' \rightarrow \bar{f}f} = \frac{\sqrt{M_{Z'}^2 - 4m_f^2} (A_f^2 (M_{Z'}^2 - 4m_f^2) + V_f^2 (2m_f^2 + M_{Z'}^2))}{12\pi M_{Z'}^2}. \quad (\text{A.4})$$

In the universal coupling case with a heavy Z' , the sum over the SM fermions amounts to a factor of 22.5, which includes 3×6 quark contributions, 3 charged lepton contributions and $3 \times 1/2$ neutrino terms. The branching ratio for the $Z' \rightarrow e^+e^-$ decay approaches $1/23.5$ in this limit.

The t -channel $Z'Z' \rightarrow \bar{\chi}\chi$ analytical results can be found in [39], which we have also reproduced.

References

- [1] S. Dodelson and L. M. Widrow, Phys. Rev. Lett. **72**, 17 (1994).
- [2] L. J. Hall, K. Jedamzik, J. March-Russell and S. M. West, JHEP **03**, 080 (2010).
- [3] O. Lebedev, JCAP **02**, 032 (2023).
- [4] O. Lebedev and J. H. Yoon, JCAP **07**, no.07, 001 (2022).
- [5] F. Koutroulis, O. Lebedev and S. Pokorski, JHEP **04**, 027 (2024).
- [6] S. Hannestad, Phys. Rev. D **70** (2004), 043506.
- [7] C. Cosme, F. Costa and O. Lebedev, Phys. Rev. D **109**, no.7, 075038 (2024).
- [8] P. Langacker, Rev. Mod. Phys. **81** (2009), 1199-1228
- [9] G. Arcadi, Y. Mambrini, M. H. G. Tytgat and B. Zaldivar, JHEP **03** (2014), 134.
- [10] O. Lebedev and Y. Mambrini, Phys. Lett. B **734** (2014), 350-353.
- [11] G. Arcadi, Y. Mambrini and F. Richard, JCAP **03** (2015), 018
- [12] C. Cosme, F. Costa and O. Lebedev, JCAP **06** (2024), 031.
- [13] C. Cosme, M. Dutra, S. Godfrey and T. R. Gray, JHEP **09** (2021), 056
- [14] P. Gondolo and G. Gelmini, Nucl. Phys. B **360** (1991), 145-179
- [15] N. Koivunen, O. Lebedev and M. Raidal, [arXiv:2403.15533 [hep-ph]].
- [16] G. Arcadi, F. Costa, A. Goudelis and O. Lebedev, JHEP **07** (2024), 044.
- [17] G. Bélanger, F. Boudjema, A. Goudelis, A. Pukhov and B. Zaldivar, Comput. Phys. Commun. **231**, 173-186 (2018).
- [18] G. Alguero, G. Belanger, F. Boudjema, S. Chakraborti, A. Goudelis, S. Kraml, A. Mjallal and A. Pukhov, Comput. Phys. Commun. **299**, 109133 (2024).
- [19] J. Silva-Malpartida, N. Bernal, J. Jones-Pérez and R. A. Lineros, [arXiv:2408.08950 [hep-ph]].
- [20] K. m. Cheung, Phys. Lett. B **517** (2001), 167-176
- [21] J. Alcaraz *et al.* [ALEPH, DELPHI, L3, OPAL and LEP Electroweak Working Group], [arXiv:hep-ex/0612034 [hep-ex]].
- [22] S. Schael *et al.* [ALEPH, DELPHI, L3, OPAL and LEP Electroweak], Phys. Rept. **532** (2013), 119-244
- [23] A. Falkowski and K. Mimouni, JHEP **02** (2016), 086
- [24] G. Aad *et al.* [ATLAS], Phys. Lett. B **796** (2019), 68-87
- [25] J. Alwall, R. Frederix, S. Frixione, V. Hirschi, F. Maltoni, O. Mattelaer, H. S. Shao, T. Stelzer, P. Torrielli and M. Zaro, JHEP **07** (2014), 079.

- [26] T. Bandyopadhyay, G. Bhattacharyya, D. Das and A. Raychaudhuri, Phys. Rev. D **98** (2018) no.3, 035027
- [27] G. Arcadi, D. Cabo-Almeida, M. Dutra, P. Ghosh, M. Lindner, Y. Mambrini, J. P. Neto, M. Pierre, S. Profumo and F. S. Queiroz, [arXiv:2403.15860 [hep-ph]].
- [28] A. Airapetian *et al.* [HERMES], Phys. Rev. D **75** (2007), 012007
- [29] J. Aalbers *et al.* [LZ], Phys. Rev. Lett. **131** (2023) no.4, 041002
- [30] E. Aprile *et al.* [XENON], Phys. Rev. Lett. **121**, no.11, 111302 (2018).
- [31] J. Billard, M. Boulay, S. Cebrián, L. Covi, G. Fiorillo, A. Green, J. Kopp, B. Majorovits, K. Palladino and F. Petricca, *et al.* Rept. Prog. Phys. **85**, no.5, 056201 (2022).
- [32] E. Aprile *et al.* [XENON], JCAP **11**, 031 (2020).
- [33] J. Aalbers *et al.* [DARWIN], JCAP **11**, 017 (2016).
- [34] T. Hambye, M. H. G. Tytgat, J. Vandecasteele and L. Vanderheyden, Phys. Rev. D **98**, no.7, 075017 (2018).
- [35] K. K. Boddy, K. Freese, G. Montefalcone and B. Shams Es Haghi, [arXiv:2405.06226 [hep-ph]].
- [36] X. R. Wong and K. P. Xie, Phys. Rev. D **108** (2023) no.5, 055035
- [37] A. McDaniel, M. Ajello, C. M. Karwin, M. Di Mauro, A. Drlica-Wagner and M. A. Sánchez-Conde, Phys. Rev. D **109** (2024) no.6, 063024
- [38] A. Berlin, D. Hooper and S. D. McDermott, Phys. Rev. D **89** (2014) no.11, 115022
- [39] M. Klasen, F. Lyonnet and F. S. Queiroz, Eur. Phys. J. C **77** (2017) no.5, 348